NUMERICAL INVESTIGATION ON THE LIQUID SLOSHING DAMPING INSIDE A TANK WITH A FLEXIBLE ANTI-SLOSHING DEVICE

F. Rossetti¹¹, L. Pirillo²¹, M. Cimini³², M. Bernardini⁴¹ & F. Stella⁵¹

Abstract

In this study, a numerical investigation, through a fluid-structure-interaction (FSI) approach, of the behavior of the lateral liquid sloshing inside a tank with a flexible anti-sloshing device (ASD), under normal gravity, is presented. The considered geometry is a rectangular tank, partially filled with water, and equipped with two ASDs on the lateral walls. A partitioned two-way FSI procedure is developed, and used to carry out a parametric analysis to investigate the influence of the ASDs' flexibility on the liquid motion damping. The results show that, increasing the ASD's flexibility, it is possible to raise the damping ratio with respect to the one obtained with a rigid device, allowing to design lighter baffles for a required level of damping.

Keywords: Fluid-structure interaction, sloshing, VOF, CFD, CSD

1. Introduction

Sloshing is the movement of the unrestrained free surface of the liquid contained in a partially filled tank, caused by the motion or excitation of its container. In particular, the liquid motion which takes place mostly in response to translational or pitching motions of the reservoir is indicated as lateral sloshing [1]. Sloshing is a phenomenon that occurs in various fields, among which oil & gas and aerospace. In particular, the latter sector has highly emphasized research into sloshing problems, driven by the need to develop high-speed aircraft and large rockets [2, 3, 4, 5]. Indeed, the sloshing motion generates forces and moments which can significantly impact the dynamics and stability of aerospace vehicles, and which can also jeopardize tank structures.

In order to mitigate sloshing inside tanks, ASDs, such as baffles, are commonly used. Baffles are partitions employed to divide the tank into compartments, stabilizing and containing the liquid within its designated areas. Baffles act as dampers of the fluid motion, and, in their presence, the liquid damping is the sum of two contributions, a smooth-wall viscous damping, which is due to the interaction between the fluid and the tank wall, and a damping due to the presence of the baffles. The first contribution is negligible with respect to the second, as it has been noticed both in experimental and numerical studies [6, 9].

Flexible baffles can be used to increase the liquid damping effectiveness, this possibility has been demonstrated experimentally [7, 8]. Such improvement depends both on the baffle depth and on the sloshing amplitude. In particular, in Garza [8], it has been seen that the rigid baffle is more effective in proximity of the free surface, instead the flexible baffles become more effective for higher baffle depths. Moreover, in Garza [8], the relative damping (ratio between the flexible baffle damping and the

¹ Department of Mechanical and Aerospace Engineering, Sapienza University of Rome, via Eudossiana 18, Rome (RM), 00184, Italy

²Laboratory of Sustainable Combustion and Advanced Thermal and Thermodynamic Cycles, ENEA, Via Anguillarese 301, 00123, Rome, Italy

¹f.rossetti@uniroma1.it

²lorenzo.pirillo@uniroma1.it

³matteo.cimini@enea.it

⁴matteo.bernardini@uniroma1.it

⁵fulvio.stella@uniroma1.it

rigid baffle damping) has been shown to vary from an approximate value of 2 for the smallest tested tank amplitude, to a value slightly greater than 1 for the highest tested tank amplitude. However, from this experimental campaign, it has remained questionable whether the flexible baffles would offer more damping than the rigid ones for larger excitations amplitudes.

Due to the cost and the complexity associated with performing experiments of sloshing with flexible ASDs (and the complexity of the operations is even increased if the liquid considered is cryogenic, as it often happens in aerospace applications), computational FSI offers a valuable alternative for studying this phenomenon. Computational FSI has been applied to several engineering scenarios, spanning from energy [16, 17] and aerospace applications [13, 14, 15], up to the medical field [18, 19]. However, its application to the sloshing in tanks with deformable baffles remains limited. Some of the studies available, in the literature, rely on the use of particle-based methods for FSI [20, 21].

Three main classes of FSI coupling techniques have been developed over the years: the field elimination treatment, the monolithic treatment, and the partitioned treatment. The application of the first methodology is advisable for linear problems. In the monolithic treatment, the governing equations for the fluid, structure, and mesh motion are solved simultaneously. The advantage of using this approach is that it is more robust; while, its disadvantage is that it requires writing a unique FSI solver, prohibiting the usage of commercial fluid and structure solvers. Instead, in the partitioned treatment, the equations of fluid mechanics, structural mechanics, and mesh motion are solved sequentially. The partitioned approach offers the appealing advantages of software reuse, and modularity, which have contributed to the selection of this approach for the present study. Nevertheless, this approach requires careful implementation to prevent significant deterioration of stability and accuracy [10].

In the present study, we have set up a partitioned two-way FSI methodology to numerically assess the possibility of increasing the liquid damping ratio in tanks with lateral sloshing, by the use of flexible ASDs. The considered test case consists of a rectangular tank, partially filled with water, and equipped with two baffles, each wedged on a side of the lateral wall. The tank wall is considered rigid, except for the baffles, for which a parametric study has been carried out, spanning different values of the Young's modulus and, hence, of the material flexibility. The interest in increasing the baffles damping stems from the desire to use lighter devices. The engineering problem considered is characterized by a strong coupling between the fluid and structural dynamics and, therefore, in the following, guidelines are given to the reader on useful techniques to stabilize the coupled solution.

The study is organized as follows: firstly, the considered geometry and operating conditions are described; after that, the details of the chosen setups for the fluid dynamics field, structural field and system coupling are specified; then the characteristics of the used meshes for the fluid dynamics and structural fields are presented; finally, the results of the analysis are outlined.

2. Computational setup

2.1 Tank geometry and Operating Conditions

The considered tank, whose geometry details are represented in Fig. 1, and summarized in Tab. 1, has a rectangular parallelepiped shape, characterized by the following dimensions: a height, H, of 1.2~m, a width, 2L, of 0.8~m, and a thickness, w, of 0.2~m. Moreover, it is equipped with two baffles, also schematized in Fig. 1, each anchored on one of the two side walls, at a height $h_b = 0.78~m$ from the tank bottom. The geometrical features of the baffles, summarized in Tab. 2, are a length, L_b , of 0.11~m, a width, w_b , of 0.16~m, and a thickness, t_b , of 3.05~mm. It is worth noticing that $w > w_b$, for this reason two gaps exist between the baffle and the front and back walls of the container. The baffles are, then, anchored only to the tank lateral walls, and behave as single edged beams.

	Value [m]	
Н	1.2	
L	0.4	
W	0.2	
h_b	0.78	

Table 1 - Tank geometrical features.

	Value [m]
w_b	0.16
L_b	0.11
t_b	$3.05 \cdot 10^{-3}$

Table 2 – Baffle geometrical features.

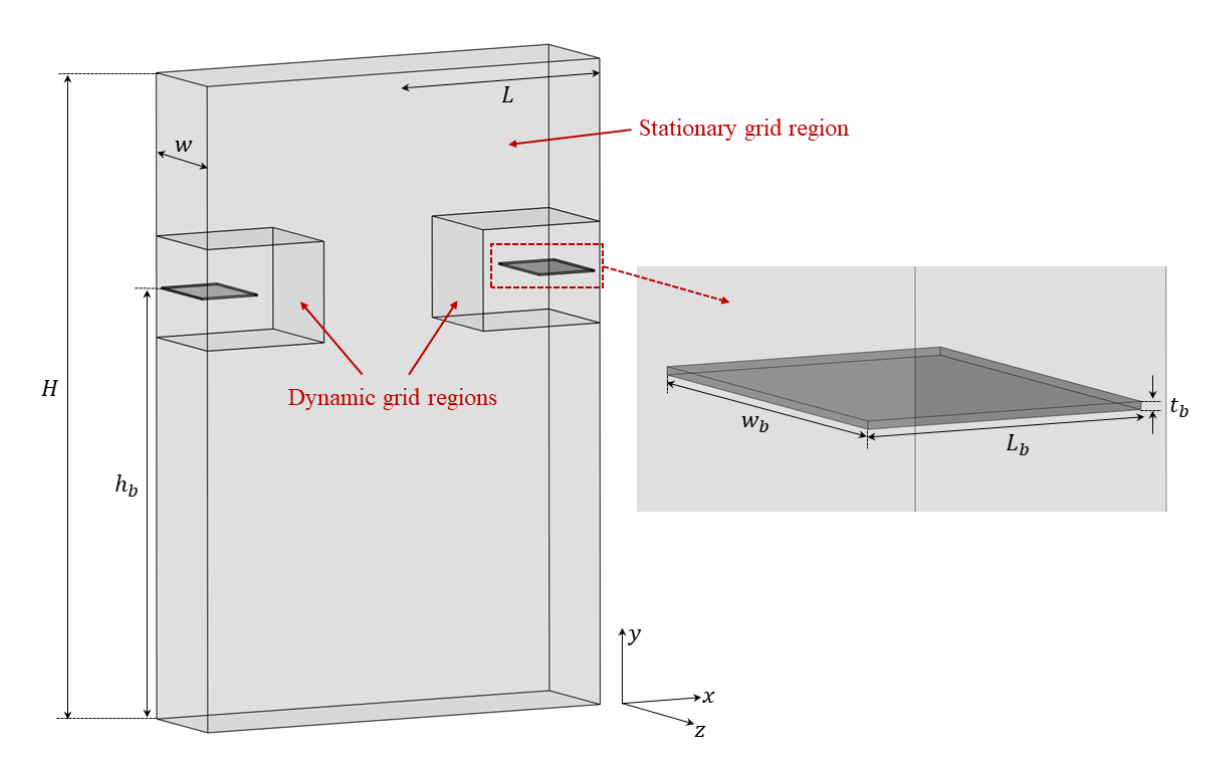


Figure 1 – Geometrical features of the tank and the baffle.

The tank is partially filled with water, having a height, h, of 0.88~m, thus, the corresponding filling level is h/L=2.23. The water is characterized by a density of $998.2~kg/m^3$ and a dynamic viscosity of $1.003 \cdot 10^{-3}~Pa \cdot s$. The ullage is filled with air, having a density of $1.225~kg/m^3$ and a dynamic viscosity of $1.79 \cdot 10^{-5}~Pa \cdot s$. The pressure inside the tank is 1~atm. The sloshing is triggered by an impulsive lateral acceleration. The magnitude of the impulse is $2~m/s^2$, its duration is 0.1~s, and it acts between 0.05~s and 0.15~s. As regards the ASD material, six different cases have been considered, which are characterized by different values of material flexibility. The values of Young's modulus, E_b , and density, ρ_b , of the baffle material, for the different cases, are summarized in Tab. 3.

Run number	FSI	$E_b[Pa]$	$\rho_b[kg/m^3]$
Run 1	Off	∞	[-]
Run 2	On	$2.1\cdot10^{11}$	2770
Run 3	On	$7.1 \cdot 10^{10}$	2770
Run 4	On	$2.4\cdot10^{10}$	2770
Run 5	On	$1.1 \cdot 10^{9}$	950
Run 6	On	$5.5\cdot10^8$	950

Table 3 – Baffles material properties for the different cases considered in the parametric study.

The selected approach has been to start from a rigid baffle configuration, in which the Young's modulus is assumed to be infinite $(E_b = \infty)$, and, then, to gradually reduce its value, in order to see the effect of material flexibility on the liquid damping ratio. In particular, the values of E_b and ρ_b associated to the simulations addressed as $Run\ 3$ and $Run\ 5$, in Tab. 3, correspond, respectively, to the choice of aluminum alloy and polyethylene, as baffle material. Instead, in the simulations addressed as $Run\ 2$, $Run\ 4$, and $Run\ 6$, the used material is fictitious as the Young's modulus has been varied either with respect to that of aluminum or with respect to that of polyethylene to investigate the effect of the material flexibility. More specifically, in $Run\ 2$, the Young's modulus is three times that of aluminum, in $Run\ 4$, it is one-third that of aluminum, and, in $Run\ 6$, it is half that of polyethylene. Moreover, the scenario characterized by an infinitely rigid baffle has not been run with a FSI approach, as only the fluid dynamics solution is significant in this case.

2.2 Fluid dynamics settings

The three-dimensional unsteady Navier-Stokes (NS) equations have been solved using the commercial CFD software Ansys Fluent[®] [11]. The Volume-of-fluid (VOF) method [24] has been used to track the two-phase fluid interface. The two phases have been modeled as incompressible, laminar, with constant thermophysical properties, and immiscible. The surface tension within the two phases has been taken into account with the Continuum Surface Force (CSF) model [25], and has been set to the constant value of 0.074N/m. For all the simulations, the pressure-based solver has been employed, with the selection of the SIMPLE algorithm as pressure-velocity coupling scheme. Second order upwind schemes have been used for spatial discretization of the convective terms in continuity and momentum equations, and Ansys Fluent[®]'s "Compressive" scheme [11] has been chosen for the volume fraction equation, with the selection of sharp interface regime modeling. A second-order implicit time discretization has been used, and the time step has been set to $0.005\ s$. Both the tank walls and the baffles walls have been considered adiabatic and no slip.

The chosen fluid dynamics setup has been validated in our previous work [9], where the experimental campaign of Perez et al. [6] has been reproduced, simulating the sloshing in a cylindrical tank with a single rigid ASD ring, for three different filling levels, and damping values comparable to the experimental ones have been obtained. With respect to the validated setup, the present one differs only for the activation of the dynamic mesh settings. Hence, in the presence of a deformable baffle, the mesh has to deform, during the computation, due to the motion of the fluid-solid interface in response to the displacements computed from the structural solver. The mesh motion has been applied only to the two parallelepiped regions confining the baffles (which are specified in Fig. 1), instead the rest of the mesh has been modeled as stationary, in order to reduce the computational time. The selected dynamic mesh method is the diffusion smoothing [11], in which the mesh motion is governed by a diffusion equation, and the mesh nodes move in response to the motion of the fluid-solid interface but do not change in number in time.

2.3 Structural dynamics settings

The selected structural solver is Ansys Mechanical[®] [12]. The structural solver, at every time step, receives the forces from the CFD solver, and computes the displacements associated to those forces. Moreover, geometric non-linearities are taken into account in the solution process.

For the present analysis, no substeps have been employed, indeed the analysis has a time step size equal to the fluid dynamics one (0.005 s).

Even if the damping of the structure is very limited compared to the fluid damping, in some of the simulations carried out (*Run* 4 , *Run* 5 , *Run* 6), the structural damping has been introduced in order to stabilize the solution process. Anyway, some of our preliminary analyses have shown that the introduction of damping in the solid, being very limited, has no effect on the damping level of the liquid. In the present study, the Rayleigh damping model [26] has been applied. In the latter formulation, the damping matrix is assumed to be proportional to the mass, and stiffness matrices. Moreover, the approach to extract the Rayleigh damping coefficients from modal analysis, proposed in [27], has been used. More specifically, the two modes corresponding to the maximum effective mass participation have been selected, and a damping ratio of 2% and 8% has been assigned to them. Moreover, even if the solid damping has been used also in *Run* 5 and *Run* 6, it was not necessary in those cases, because the coupled solution was already stabilized by the application of the interface quasi-Newton with inverse Jacobian from a least-squares (IQN–ILS) model. Finally, the boundary condition applied to the side of the structure attached to the wall is that of a fixed support, i.e. all the degrees of freedom (both translations and rotations) are set as null on that boundary.

2.4 Systems coupling settings

A partitioned two-way FSI procedure has been implemented using Ansys System Coupling[®] [28]. Since two-way FSI simulations have been carried out, two data transfers exist. The first one is represented by the transmission of force data from the CFD solver to the CSD one. On the other hand, the second data transfer arises when the CSD solver transfers back to the CFD one the displacements associated with the external loads. Such displacements serve as an input for the process of mesh movement.

The FSI iterations inside a coupling step are carried out until data transfer convergence is reached, i.e. when the root mean square, over all locations, of the normalized change in the data transfer value between two successive iterations is equal to a convergence target (here set to 0.01), or when the maximum number of coupling iterations, N_{max} , is reached.

Moreover, to improve the convergence of the analysis, in the cases characterized by a high value of the baffle material flexibility, the force computed from the fluid dynamics solver is transferred to the solid domain using the ramping procedure. More specifically, the entire fluid dynamics force is not transferred instantaneously to the solid domain, at the beginning of each coupling step. Instead, in each coupling step, the force value transferred to the solid side of the interface is increased linearly to the overall value, in a certain number of iterations, N_{min} . A schematic of the ramping procedure used for the force data transfer is shown in Fig. 2.

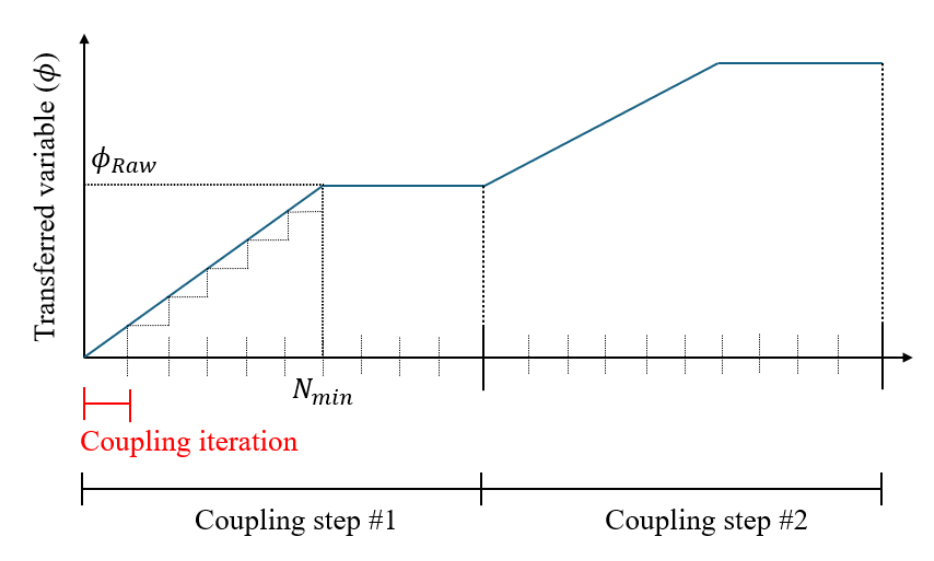


Figure 2 – Schematics of the ramping procedure for data transfer: transferred variable as a function of the coupling iteration.

In some cases, i.e. when the baffle is highly deformable, reaching a converged FSI solution can be challenging. Indeed, the baffle is a slender body moved by an incompressible fluid in a non-stationary motion, and, in addition, the density of the solid is comparable with the fluid one when polyethylene is used, causing a significant added mass effect. In those cases, the IQN–ILS [22, 23] has been used to stabilize and accelerate the coupled solution. When using this model, an approximate Newton iteration is applied to the data transferred at the coupling interface [22, 23]. The settings used for the systems coupling for the various cases considered are summarized in Tab. 4.

Run number	Ramping	IQN-ILS	N_{max}	N_{min}
Run 1	Off	Off	5	[-]
Run 2	Off	Off	5	[-]
Run 3	Off	Off	5	[-]
Run 4	Off	Off	5	[-]
Run 5	On	On	12	5
Run 6	On	On	12	5

Table 4 – Systems coupling settings.

2.5 Meshing strategy

For the fluid domain, a fully polyhedral mesh (of average size $\Delta s_{body} = 0.06~m$), with a volumetric refinement (of average size $\Delta s_{surf} = 0.01~m$) in the region containing the baffles and the liquid free surface, has been chosen. A three-dimensional view of the fluid grid is shown in Fig. 3.

Concerning the solid domain, a fully structured hexahedral mesh (of medium size $\Delta s_{solid} = 1.6 \cdot 10^{-3} m$) has been adopted.

Numerical Investigation on the Liquid Sloshing Damping inside a Tank with a flexible Anti-sloshing device

The features of both meshes are summarized in Tabs. 5 and 6. The two grids are non-matching at the fluid/solid interface, as it is evident in Fig. 4, which shows the surface grids at the interface, on the fluid side (left) and on the solid side (right).

	Value
Number of cells	$1 \cdot 10^5$
Δs_{surf} [m]	0.01
Δs_{body} [m]	0.06

Tabla	_	maah	features
iaoie	:) —	mesn	realines.

	Value
Number of cells (1 baffle)	$1.4 \cdot 10^4$
Δs_{solid} [m]	$1.6\cdot10^{-3}$

Table 6 – Solid mesh features.

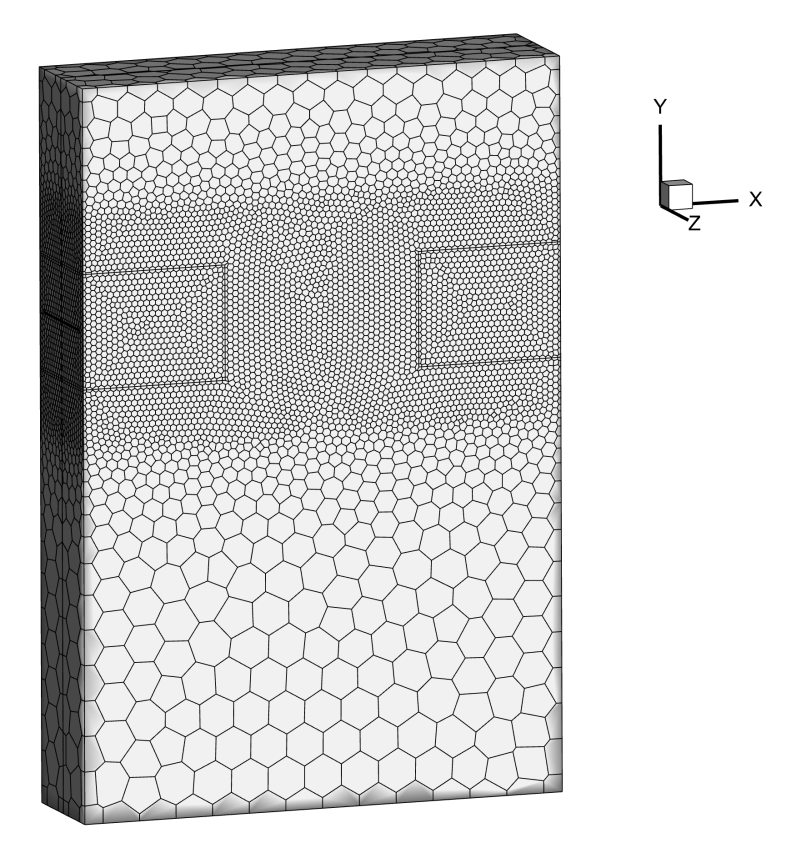


Figure 3 – Three-dimensional view of the fluid grid.

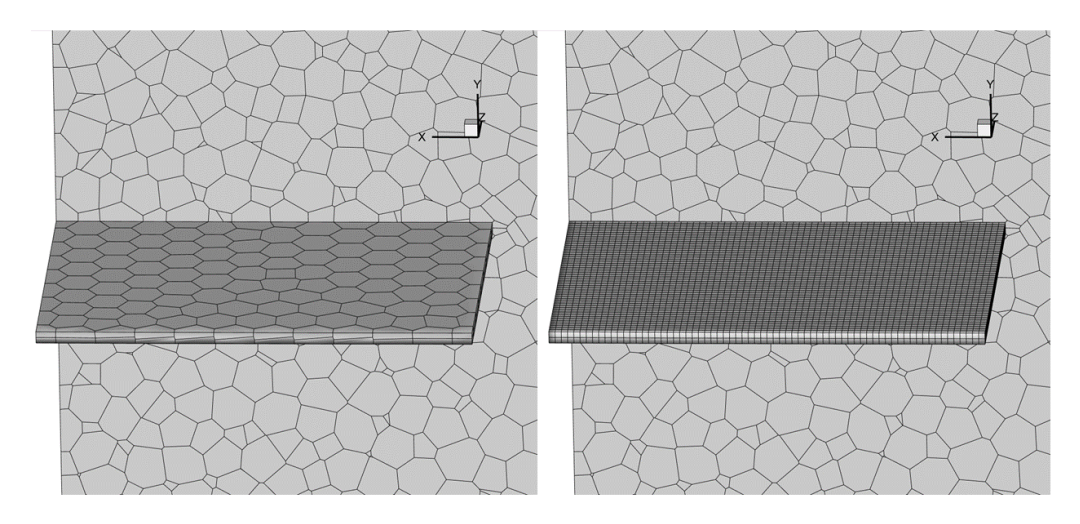


Figure 4 – Non-matching grids at the fluid/solid interface: fluid side (left) and solid side (right).

3. Results

In this section, the results obtained with the infinitely rigid ASD configuration are compared with those obtained with the materials characterized by a decreasing level of the Young's modulus, to assess the possibility of increasing the mitigation of the sloshing motion, and, consequently, of the lateral forces acting on the container's walls, when the baffle's deformability increases.

Fig. 5 shows the time history of the lateral force for the six values of Young's modulus considered in the parametric study. The lateral force represents the total force acting on the tank and baffle walls, projected in the direction of the sloshing solicitation.

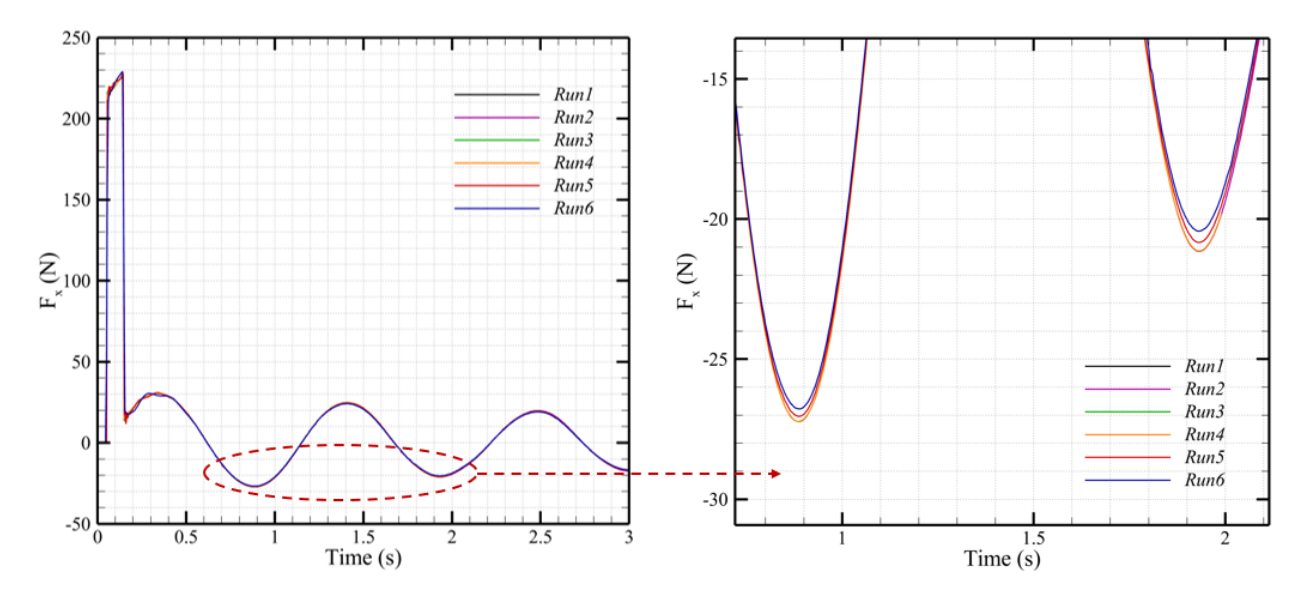


Figure 5 – Time history of the lateral force for the six cases considered in the parametric study (left), with a zoom of the region comprising the first two minima of the lateral force (right).

After the end of the lateral impulse, acting between $0.05 \ s$ and $0.15 \ s$, a damped sloshing motion begins, and an oscillating behavior in the lateral force can be observed, with a characteristic frequency of about $1 \ Hz$, for all the scenarios considered. Thus, it can be concluded that, for the analyzed configurations, the baffle flexibility does not influence the first sloshing mode frequency.

The effectiveness of suppression devices depends upon the damping forces they can provide on the liquid motion, which can be evaluated by means of the damping ratio, γ . For a free-decaying sloshing, in a fixed tank, the amplitude of the slosh oscillations decreases according to a logarithmic decrement law, so the damping ratio is defined as:

$$\gamma = \frac{1}{2\pi n} \ln \left(\frac{x_0}{x_n} \right) \tag{1}$$

where x_0 represents the amplitude of the slosh wave at a selected initial moment, and x_n represents the amplitude of the slosh wave at a selected terminal moment, after n cycles. In this work, the damping ratio has been evaluated using the first two minima of the oscillating signal of the lateral force, F_x , and so the value of n is equal to one.

The values of the damping ratio obtained for the different values of Young's modulus considered are summarized in Tab. 7.

Starting from the rigid baffle configuration, for which the damping ratio results to be $\gamma = 0.0402$, no increase in the damping ratio is observed if the Young's modulus is decreased down to the aluminum's value ($Run\ 3$). Indeed, in these cases, the maximum vertical displacement, associated to the tip of the baffle, is about $20\ \mu m$, and so the ASD deformability is negligible.

The first small effects given by the material deformability are visible when the Young's modulus is decreased to the value of $2.4\cdot 10^{10}$ Pa (Run 4). In this case, the maximum baffle displacement becomes $60~\mu m$, and the damping ratio is characterized by an increase of 0.25% with respect to the infinitely rigid case.

Numerical Investigation on the Liquid Sloshing Damping inside a Tank with a flexible Anti-sloshing device

Run number	Damping ratio	E _{r%} [%]	Max displ. [mm]
Run 1	0.0402	[-]	0.000
Run 2	0.0402	0.00	0.007
Run 3	0.0402	0.00	0.020
Run 4	0.0403	0.25	0.060
Run 5	0.0415	3.23	1.540
Run 6	0.0431	7.21	2.595

Table 7 – Results of the simulations in terms of damping ratio, percentage relative variation, $E_{r\%}$, of damping ratio with respect to the rigid case, and maximum vertical displacement of the baffle tip.

When the material chosen for the baffles is polyethylene ($E_b = 1.1 \cdot 10^9 \ Pa$), the baffle's flexibility is such that the damping ratio experiences an increase of 3.23% with respect to the rigid case, and the baffles experience a maximum vertical displacement of 1.54 mm.

Lastly, the increase in damping ratio reaches the maximum value of 7.21% if the Young's modulus is halved with respect to that of polyethylene (Run 6). Indeed, in the latter case, the baffle tip reaches about $2.6 \ mm$ in terms of maximum vertical displacement. For this case, characterized by the highest flexibility, the vertical displacement of the baffles in correspondence of two configurations of the free surface is shown, in Fig. 6. Finally, in Fig. 7, the contours of the z-vorticity on the x-y symmetry plane, for the rigid case, i.e. Run 1 (top), and for the most flexible case, i.e. Run 6 (bottom), at two instants, $0.2 \ s$ (Fig. 7 a)) and $0.4 \ s$ (Fig. 7 b)), are shown. It is evident that, in the case of flexible baffles, the vorticity in the region near the baffles is stronger, thus the vortices detaching from the ring tip are more intense, and they have a stronger interaction with the free surface, increasing the damping level.

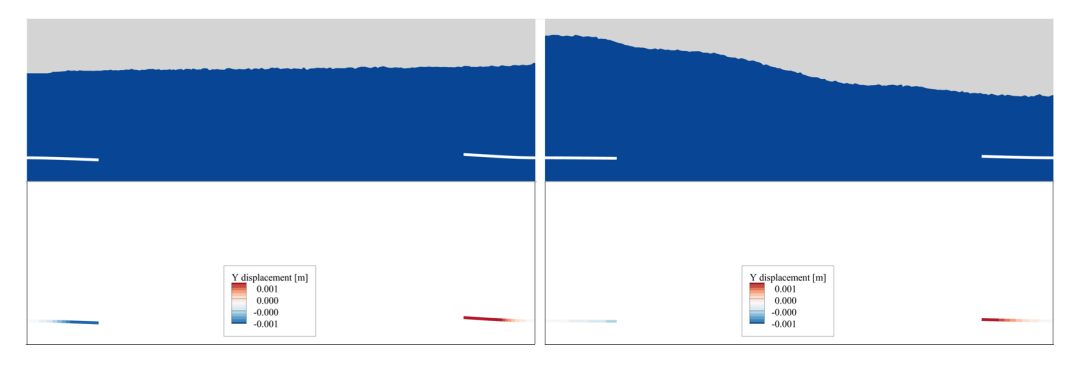


Figure 6 – Water volume fraction (top) and baffle vertical displacement (bottom) at 0.1 s (left) and 0.9 s (right). Figures refer to *Run* 6.

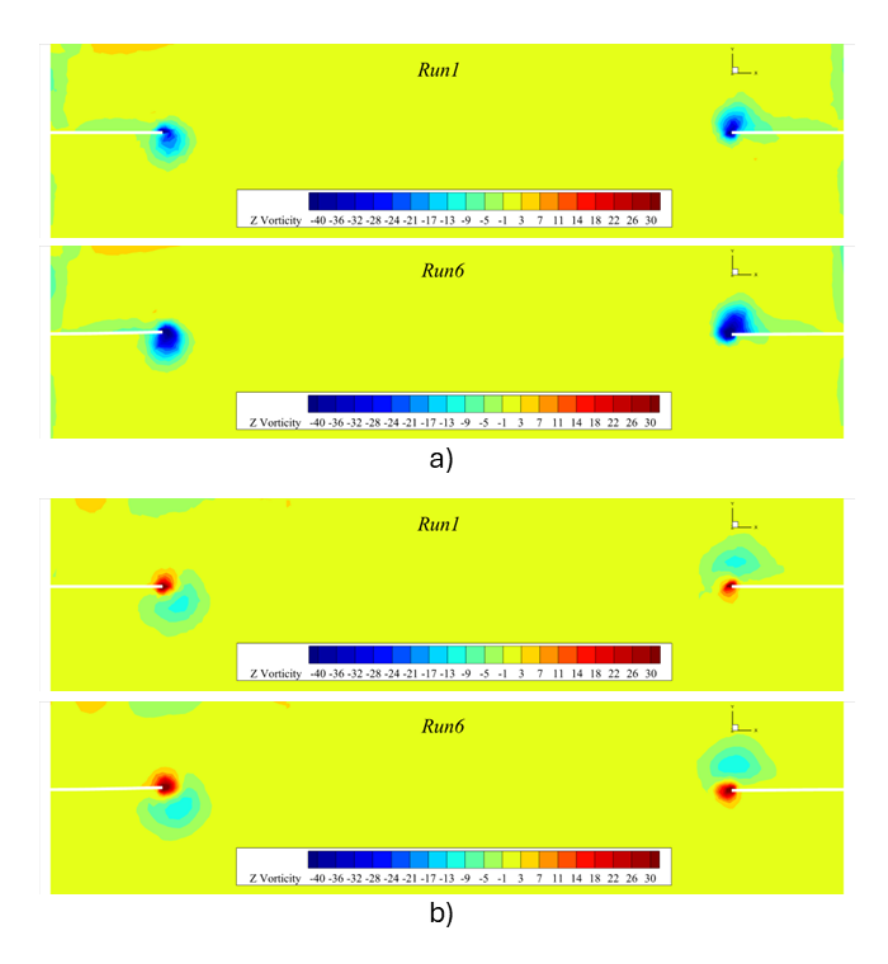


Figure 7 – Contours of the z-vorticity in the x-y symmetry plane, for $Run\ 1$ and $Run\ 6$, at a) $t=0.2\ s$ and b) $t=0.4\ s$.

4. Conclusions

In this study, a partitioned two-way FSI methodology, relying on the use of existing commercial softwares, has been developed and applied to the technological problem of lateral sloshing in tanks with deformable baffles. Moreover, a parametric study on the value of the baffles material flexibility has been carried out, while the rest of the tank wall has been modeled as rigid. The considered geometry consists of a rectangular tank, partially filled with water, and with two ASDs anchored on the lateral walls.

The results show that, for the considered geometry, fluid, baffle location below the free surface, and forcing acceleration, if the Young's modulus is decreased down to the aluminum value, no variations in terms of the damping ratio with respect to the infinitely rigid case can be noticed. On the other hand, if the Young's modulus is decreased of two orders of magnitude with respect to the aluminum value, a potential (because some of the materials considered are not real) increment of the damping ratio up to about 7% can be reached. The possibility to increase the damping ratio modifying the baffle material flexibility is appealing as it paves the way towards the production of lighter devices.

The increase of damping ratio with the material flexibility increment can be attributed to the higher mobility of the baffle in response to the liquid motion, which increases the intensity of the vortices detaching from the ring tip, and, thus, increases their interaction with the free surface.

However, the material flexibility, despite affecting the baffle damping effectiveness, does not influence the first sloshing mode frequency, for the considered operating conditions.

As concerns a methodological point of view, as the engineering problem considered is characterized by a strong FSI coupling, the use of procedures to stabilize the coupled solution is highly recommended for the cases characterized by high values of baffle flexibility. These procedures are, firstly, the ramping of the force data and, if necessary, also of the displacement data transferred between the CFD and the CSD solvers. Secondly, the use of the interface quasi-Newton with inverse Jacobian

from a least-squares model is recommended to stabilize and accelerate the coupled solution process. Finally, the objective of the ongoing and future activities is to further deepen the knowledge on the influence of flexible baffles on the sloshing behavior, in particular on the damping ratio and first sloshing mode frequency. To achieve this goal, several configurations will be considered, characterized by different geometries, fluid as well as baffle materials, baffle location below the free surface, and excitation amplitudes.

5. Copyright Statement

The authors confirm that they, and/or their company or organization, hold copyright on all of the original material included in this paper. The authors also confirm that they have obtained permission, from the copyright holder of any third party material included in this paper, to publish it as part of their paper. The authors confirm that they give permission, or have obtained permission from the copyright holder of this paper, for the publication and distribution of this paper as part of the ICAS proceedings or as individual off-prints from the proceedings.

Acknowledgments

This work is part of the research activity developed by the authors within the framework of the "PNRR" CN4 MOST (Mobilità sostenibile): SPOKE 1 (Air Mobility), WP5: "Multidisciplinary design optimization and innovative solutions for next generation green aircraft with demonstrator".

References

- [1] Abramson, H. N. The dynamic behavior of liquids in moving containers, with applications to space vehicle technology. NASA SP-106, 1966.
- [2] Schy, A. A. A theoretical analysis of the effects of fuel motion on airplane dynamics. National Advisory Committee for Aeronautics, Vol. 1080, 1951.
- [3] Sewall, J. L. An experimental and theoretical study of the effect of fuel on pitching-translation flutter, 1957.
- [4] Abramson, H. N. and Garza, L. R. *Liquid frequencies and damping in compartmented cylindrical tanks.* Journal of Spacecraft and Rockets, Vol. 2, No. 3, pp 453-455, 1965.
- [5] Bauer, H. F. *Theory of fluid oscillations in partially filled cylindrical containers*. MSFC, Rept. No. MTP-AERO-62-1,(Jan. 1962), Vol. 4, 1962.
- [6] Perez, J. G., Parks, R., and Lazor, D. R. Validation of slosh model parameters and anti-slosh baffle designs of propellant tanks by using lateral slosh testing. 28th Aerospace Testing Seminar, No. M12-1999, 2012.
- [7] Stephens, D. G. *Flexible baffles for slosh damping*. AIAA journal of spacecrafts and rockets, Vol. 3, No. 5, pp 765-766, 1966.
- [8] Garza, L. R. *A comparison of flexible and rigid ring baffles for slosh suppression*. Technical report No. 1, NASA-CR-78355, 1966.
- [9] Cimini, M., Rossetti, F., Della Posta, G., Stella, F., and Bernardini, M. *CFD analysis of the lateral sloshing phenomenon inside an aerospace LH2 cryogenic tank*. Aerospace Europe Conference 2023 10th EUCASS 9th CEAS, 2023.
- [10] Felippa, C. A., Park, K. C., and Farhat, C. *Partitioned analysis of coupled mechanical systems*. Computer methods in applied mechanics and engineering, Vol. 190, pp 3247-3270, 2001.
- [11] Ansys Fluent Documentation. Release 2021 R2, 2021.
- [12] Ansys Mechanical Documentation. Release 2021 R2, 2021.
- [13] Takizawa, K., Spielman, T., and Tezduyar, T. E. Space-time FSI modeling and dynamical analysis of spacecraft parachutes and parachute clusters. Computational Mechanics, Vol. 48, No. 3, pp 345-364, 2011.
- [14] Farhat, C., Van der Zee, K. G., and Geuzaine, P. *Provably second-order time-accurate loosely-coupled solution algorithms for transient nonlinear computational aeroelasticity.* Computer methods in applied mechanics and engineering, Vol. 195, No. 17-18, pp 1973-2001, 2006.
- [15] Lesoinne, M. and Farhat, C. *Higher-order subiteration-free staggered algorithm for nonlinear transient aeroelastic problems.* AIAA journal, Vol. 36, No. 9, pp 1754-1757, 1998.
- [16] Agamloh, E. B., Wallace, A. K., and Von Jouanne, A. *Application of fluid-structure interaction simulation of an ocean wave energy extraction device.* Renewable Energy, Vol. 33, No. 4, pp 748-757, 2008.

Numerical Investigation on the Liquid Sloshing Damping inside a Tank with a flexible Anti-sloshing device

- [17] Khalid, S., Zhang, L., Zhang, X., and Sun, K. *Three-dimensional numerical simulation of a vertical axis tidal turbine using the two-way fluid structure interaction approach*. Journal of Zhejiang University-SCIENCE A (Applied Physics Engineering), 2013.
- [18] Reymonda, P., Crosetto, P., Deparis, S., Quarteroni, A., and Stergiopulos, N. *Physiological simulation of blood flow in the aorta: Comparison of hemodynamic indices as predicted by 3-D FSI, 3-D rigid wall and 1-D models.* Medical Engineering Physics, 2013.
- [19] Doost, S. N., Ghista, D., Su, B., Zhong, L., and Morsi, Y. S. *Heart blood flow simulation: a perspective review.* BioMedical Engineering OnLine, 2016.
- [20] Hwang, S. C., Park, J. C., Gotoh, H., Khayyer, A., and Kang, K. J. *Numerical simulations of sloshing flows with elastic baffles by using a particle-based fluid-structure interaction analysis method.* Ocean engineering, Vol. 118, pp 227-241, 2016.
- [21] Yang, C., Zhang, H., Su, H., and Shen, Z. *Numerical simulation of sloshing using the MPS-FSI method with large eddy simulation.* China Ocean Engineering, 2018.
- [22] Degroote, J., Bathe, K. J., and Vierendeels, J. *Performance of a new partitioned procedure versus a monolithic procedure in fluid–structure interaction.* Computers & Structures, Vol. 87, No. 11-12, pp 793-801, 2009.
- [23] Degroote, J., Haelterman, R., Annerel, S., Bruggeman, P., and Vierendeels, J. *Performance of partitioned procedures in fluid–structure interaction.* Computers & structures, Vol. 88, No. 7-8, pp 446-457, 2010.
- [24] Hirt, C. W. and Nichols, B.D. *Volume of fluid (VOF) method for the dynamics of free boundaries.* Journal of Computational Physics, Vol. 39, No. 1, pp 201-225, 1981.
- [25] Brackbill, J. U., Kothe, D. B., and Zemach, C. *A continuum method for modeling surface tension.* Journal of Computational Physics, Vol. 100, No. 2, pp 335-354, 1992.
- [26] Rayleigh, J. W. S. The theory of sound. Vol. 1, Dover Pub., New York, 1877.
- [27] Rahul, B., Dharani, J., and Balaji, R. *Optimal method for determination of Rayleigh damping coefficients for different materials using modal analysis.* International Journal of Vehicle Structures & Systems, Vol. 13, No. 1, pp 102-111, 2021.
- [28] ANSYS System Coupling Documentation. Release 2021 R2. 2021.